https://doi.org/10.1016/j.nanoen.2019.103943

A low-frequency, broadband and tri-hybrid energy harvester with septuple-stable nonlinearity-enhanced mechanical frequency up-conversion mechanism for powering portable electronics

Chen Wang[a], Siu-Kai Lai[a,b,*], Zhi-Chong Wang[c], Jia-Mei Wang[a], Weiqing Yang[d], Yi-Qing Ni[a,b]

[a] *Department of Civil and Environmental Engineering, The Hong Kong Polytechnic University, Kowloon, Hong Kong, P.R. China*

[b] *Hong Kong Branch of National Rail Transit Electrification and Automation Engineering Technology Research Center, The Hong Kong Polytechnic University, Kowloon, Hong Kong, P.R. China*

[c] *Tianjin Key Laboratory of Nonlinear Dynamics and Control, Department of Mechanics, School of Mechanical Engineering, Tianjin University, Tianjin, 300072, P.R. China*

[d] *Key Laboratory of Advanced Technologies of Materials (Ministry of Education), School of Materials Science and Engineering, State Key Laboratory of Traction Power, Southwest Jiaotong University, Chengdu, 610031, P.R. China*

Abstract

This study involves the design and investigation of a low-frequency, broadband, tri-hybrid energy harvester. The harvester consists of a novel septuple-stable nonlinearity-enhanced mechanical frequency up-conversion mechanism that not only enhances the output performance of the frequency up-conversion via inter-well motions, and also offers a wide and highly efficient operating bandwidth at low acceleration via the combination of resonant inter-well oscillation behavior and non-resonant behavior. The integration of an impact-driven piezoelectric generator, an electromagnetic generator, and a freestanding-mode triboelectric nanogenerator allows more energy to be harvested from a single mechanical motion, which further improves the power density. A prototype is fabricated and demonstrated using an electrodynamic shaker and various human motions. In the electrodynamic shaker test, the prototype exhibits a broad bandwidth of 2–12.5 Hz and generates an output power of 24.17 mW, corresponding to a power density of 700.3 W/m^3 across a matching load resistance of 35 kΩ at a frequency of 5 Hz and 1 g acceleration. Under various basic human motions such as handshaking, walking, and slow running, the prototype can generate output powers of 38.5, 24.5, and 27.2 mW, respectively, in horizontal positions and 42.7, 10.2, and 33.1 mW, respectively, in vertical positions. A comparison study is also presented to demonstrate that the tri-hybrid prototype can

*Corresponding author. *E-mail address*: sk.lai@polyu.edu.hk

produce a much higher power density than other devices reported recently. This work makes significant progress toward hybrid-energy harvesting from various human motions and its potential application in powering wearable devices.

Keywords: Tri-hybrid energy harvester, Septuple-stable nonlinearity, Frequency up-conversion, Piezoelectric generator, electromagnetic generator, Triboelectric nanogenerator

1. Introduction

With the ongoing development of wireless sensor networks and portable electronic devices, the need for sustainable mobile power supplies has grown. These devices and sensors are mainly powered by conventional electrochemical batteries or micro-fuel cells, which are limited in lifespan, chemically hazardous, bulky, costly, and complicated to replace. To address these shortcomings, recent efforts have been made to develop built-in energy harvesters to realize self-powered wireless sensors and portable electronic devices [1, 2]. As a result, various kinds of energy harvesters have been developed to generate the required electricity by converting ambient energy sources such as vibration, solar, thermal, biochemical, acoustic noise, and radio waves [3, 4]. In particular, vibration energy sources are the most attractive due to their versatility, incorruptibility, and pervasiveness [5, 6]. Various mechanisms that have been extensively exploited to harvest vibration energy include piezoelectric [7–11], electromagnetic [12–15], electrostatic [16, 17], and triboelectric [18–28] approaches. Each mechanism generates electrical power by coupling the applied vibration or motion to a mechanical structure with transducer elements.

Most ambient vibration sources around us are low-frequency, random, and time-varying. In particular, human body-induced vibration-based applications desirable for powering wearable electronic devices are also characterized by low frequencies (less than 10 Hz) and large amplitudes [29]. Generally, it is challenging to harvest energy from such a low-frequency vibration source because the power generation of a vibration energy harvester decreases dramatically at low frequencies [30, 31]. Moreover, most vibration energy harvesters are resonant-based and must therefore be quite large to match the low frequencies. Although non-resonant harvesters are not bothered by this issue, they cannot benefit from the magnified factor of resonance when they work under a periodic vibration [32]. For these reasons, the power generation of energy harvesters alone remains quite low and is not enough to power portable electronic devices, particularly under the operating conditions of low-intensity and low-frequency human motions [33].

By hybridizing multiple transduction mechanisms, more electricity can be harvested from a single mechanical movement, and the advantages of different transduction mechanisms can be taken in one package [2]. Inspired by this idea, intensive studies of bi-hybrid generators with hybrid mechanisms such as piezoelectric–electromagnetic [34–38], electromagnetic–triboelectric [33, 39–45], and piezoelectric–triboelectric [46–48] have been carried out to improve the overall power output at low frequencies. Although these works are very innovative and interesting, sustainably powering commercial portable electronic devices or sensors by low-intensity human motion alone remains a challenge. One direct solution of this issue is to hybridize more transduction mechanisms in a single

mechanical movement. A piezoelectric–electromagnetic–triboelectric hybrid energy harvester was first proposed in Ref. [49]. However, because of its complex structural design, this tri-hybrid energy harvester did not significantly improve power generation. Coupling low-frequency vibration (generated by human motion) into the triple transducer elements of the generator requires an optimized design solution.

Mechanical frequency up-conversion is another mainstream approach for high-efficiency energy harvesting in low-frequency applications [50]. This approach allows the transducer elements to actuate at their own resonant frequencies (high frequencies) via a low-frequency or non-resonant oscillator that absorbs energy from basic human motions such as walking, running, handshaking, or limb movement [50–54]. However, harvesting energy with large amplitudes from low-intensity human motion is challenging because most of the harvested energy is generated during the instantaneous coupled vibration period [55]. To overcome this issue, our group proposed a quintuple-stable nonlinearity-based frequency up-conversion mechanism to improve the intensity and duration of the coupled vibration via inter-well motions. This mechanism realized broadband energy harvest from low-intensity vibration with lower frequencies and boosted the output power as much as 35 times that of a conventional counterpart [56]. However, for wearable applications, a more compact design with this mechanism is required to be developed.

Herein, a new miniaturized piezoelectric–electromagnetic–triboelectric hybrid energy harvester is proposed. This harvester is designed and developed using a novel septuple-stable nonlinearity-enhanced mechanical frequency up-conversion mechanism to power portable electronics via various human motions. The septuple-stable nonlinearity, having seven stable states, not only combines resonant inter-well oscillation behavior and non-resonant behavior to achieve high efficiency and a broad operating bandwidth to cover the low frequencies of general human-induced motions, it also significantly improves the output performance of the mechanical frequency up-conversion process via inter-well motions. Also, by integrating an impact-driven piezoelectric generator, an electromagnetic generator, and a freestanding-mode triboelectric nanogenerator, more electric power can be harvested from a single mechanical motion, which can further improve the power density. Making use of theoretical modeling and experimental analysis of the prototype, the output performance of the hybrid system is investigated in a low-frequency range corresponding to various human motions. Moreover, practical usage of the proposed harvester for charging storage units, lighting light-emitting diodes (LEDs), and powering sensors and electronic humidity/temperature meters is demonstrated. With a wider bandwidth and much higher power density than similar devices reported recently [2, 37, 39, 44, 49, 57], the designed system makes significant progress toward hybrid energy harvesting from various

human motions and its potential application for powering portable electronics.

2. Experimental section

2.1 Fabrication of the tri-hybrid generator

First, a NdFeB cuboid magnet (1.5 × 1.5 × 0.5 cm, N35 grade) with two beryllium bronze headers was put into a rectangular acrylic tube to slide as a proof mass. Two NdFeB magnets (1 × 0.4 × 0.2 cm each, N35 grade) were respectively embedded in the center of the upper and lower wells of the tube. Two pairs of flexible stoppers, each of which consists of one unimorph piezoelectric cantilever and one bimorph piezoelectric cantilever beam were symmetrically placed at both side of the acrylic tube and separated by a distance of 3 mm from the tube. Each unimorph piezoelectric cantilever beam consists of a Macro Fiber Composite (MFC) patch [M 2814 P2] mounted on a 3.3 × 2 × 0.02-cm beryllium bronze plate, while each bimorph piezoelectric cantilever beam consists of two MFC patches mounted on both sides of a 3 × 1.8 × 0.03-cm beryllium bronze plate. Four rectangular-shaped coils (300 turns each) were connected in series and attached in pairs on the upper and lower outer surfaces of the acrylic tube. The gap between the surfaces of the sliding magnet and the coil was maintained at 0.9 mm. An aluminum (Al) film 50 μm thick and 20 mm wide covered the surface of the sliding proof mass as a freestanding tribo-material. Two 50-μm-thick copper films were attached on the inner surface of the acrylic tube with a 0.1-mm gap between them; these films served as the back electrodes. A polytetrafluoroethylene (PTFE) film with a thickness of 50 μm was aligned onto the surfaces of the back electrodes as another tribo-material.

2.2. Electrical measurement and characterization

For the electrical measurement of the hybrid generator under different excitations, a proportional-integral-derivative (PID) feedback loop was implemented by using a vibration controller (SPEKTRA VCS 201) that took the feedback signal from an accelerometer (DYTRAN 3056B2) mounted on an electrodynamic shaker (SPEKTRA APS 420). The load-circuit current of the prototype was measured across load resistances of 45 and 135 kΩ for the piezoelectric generator (PEG), 290 Ω for the electromagnetic generator (EMG), and 20 MΩ for triboelectric nanogenerator (TENG). All signals were recorded and displayed on a digital oscilloscope (Tektronix DPO4104B).

3. Results and discussion

3.1. Configuration and working principle of the tri-hybrid generator

A frequency up-converted PEG, an EMG, and a sliding-mechanism TENG were optimally

integrated in a septuple-stable dynamic system as a hybrid cell, as schematically illustrated in Fig. 1. As shown in Fig. 1(b), the size of the prototype is 63 mm (length) × 28 mm (width) × 20.1 mm (effective height). The PEG mainly consisted of a slider (as a proof mass) with a central magnet and four rigid generating beams composed of MFCs and beryllium bronze plates. The slider was placed in a rectangular acrylic tube to restrain its motion to a single direction, and its interaction with two small fixing magnets embedded in the upper and lower wells of the tube acted as a magnetic spring. The two beryllium bronze headers on both ends of the slider reduced the resonant frequency and collided with the generating beams (with higher resonant frequencies) during vibration. Initially, as shown in Fig. 2(a), the slider remained stable in the middle of the tube due to the magnetic spring. The four generating beams with two kinds of configuration (distinguished as A and B) were clamped in pairs at both ends of the tube 3 mm (d_1) and 4.8 mm (d_2), respectively, from the slider. The effective length of these two kinds of generating beams were 31.2 mm (l_1) and 27.6 mm (l_2), respectively, so that the slider collided with the free end of each beam during vibration. When a human-induced vibration with significantly large acceleration amplitude was applied to the generator along the tube, the slider started to vibrate, with the headers colliding with the generating beams in turn. After collision, the slider and the generating beam(s) were subjected to coupled vibration for a short time before separation. Afterwards, each generating beam can vibrate with exponentially attenuating amplitude at its higher resonant frequency, thereby inducing the mechanical frequency up-conversion mechanism. For the MFC attached to the fixed end of the generating beam, the cyclic deformation of the generating beam can induce tension or compressive forces along the beam length direction of the MFC. Based on the piezoelectric effect [58], when the piezoelectric element is connected to an external circuit, the resultant charges are then extracted.

To enhance the energy transfer during the frequency up-conversion process and extend the operating bandwidth, a septuple-stable nonlinear characteristic was designed in the hybrid generator. This characteristic was realized by optimally combining the force of the magnetic spring and the generating beams. As illustrated in Fig. 2, if the relative displacement of the slider exceeds d_1, the slider engages and deforms the generating beam A (GBA) in the moving direction with an additional stiffness of k_1 (the effective stiffness of GBA) feedback to the slider. If the relative displacement of the slider further exceeds ($d_2 - t_e$), where t_e represents the space consumed by GBA, both generating beams get involved. The additional stiffness is increased to $k_1 + k_2$, where k_2 denotes the effective stiffness of generating beam B (GBB) during that period. Combined with the magnetic spring force, the restoring force of the generator will have 13 zero points, which denote 13 equilibrium positions, 7 of which are stable (corresponding with positions I, II,…, VII, shown in Figs. 2(a) and 2(c)). By creating a septuple-

stable nonlinear characteristic, the system can distribute its potential energy more uniformly, which provides shallower potential wells and results in a lower excitation threshold for inter-well motion. Greater deflection of the generating beams is easily achieved via inter-well oscillations between II and VI or III and VII to enhance the energy transfer in the frequency up-conversion process. In addition, owing to the presence of seven potential wells, the tri-hybrid generator has two kinds of resonant frequencies. One is around the trivial equilibria and the other is around the non-trivial equilibria. When the excitation frequency is near either of these local oscillation frequencies, resonant oscillation occurs. This broadens the operating bandwidth of the tri-hybrid generator at low frequencies, which is beneficial to energy harvesting from human body-induced vibrations.

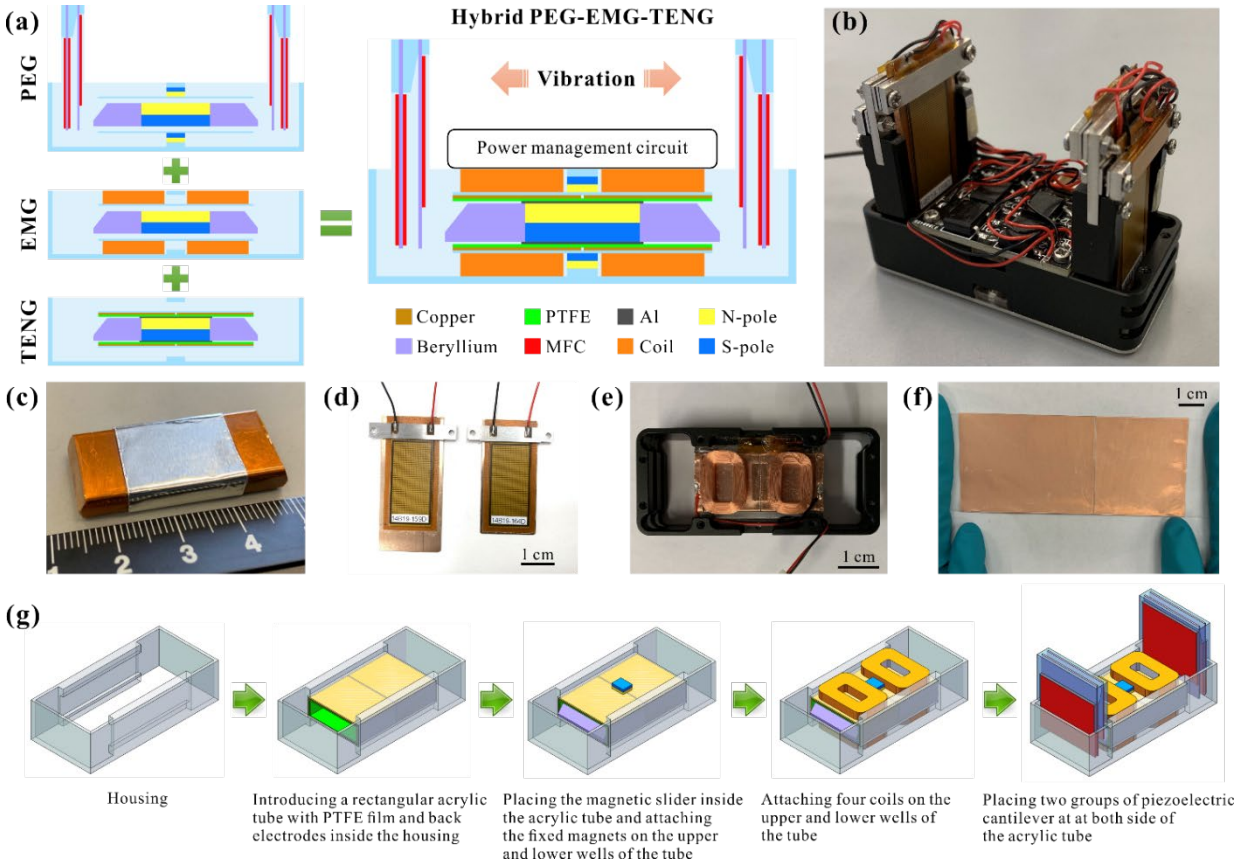

Fig. 1. (a) Schematic of the tri-hybrid energy harvester, (b) photograph of the fabricated prototype (63 mm (length) × 28 mm (width) × 20.1 mm (effective height)), (c) slider, (d) generating beams, (e) coils on one side, (f) PTFE film with Cu back electrodes, and (g) step-by-step assembly diagram of the tri-hybrid energy harvester.

For the EMG, four rectangular coils were connected in series and attached in pairs on the upper and lower outer surfaces of the rectangular tube, separated by the fixing magnets. The TENG was composed of an Al electrode covering the middle part of the slider to generate friction during vibration (Fig. 1(a)). The internal surface of the rectangular tube was attached to a PTFE film with two Cu

electrodes. According to the triboelectric series, PTFE has a higher electron affinity than Al, which results in negative triboelectric charges on the surface of PTFE film and positive triboelectric charges on the Al surface. Fig. 3 shows a schematic of the power generation process of the EMG and TENG over a half cycle (not at the very beginning of the slider vibration, but one after that), which can be separated into four stages. At the neutral position (stage i), the slider is in the center of the rectangular tube with equal negative charges on the Al electrode. Once the slider moves to the right side of the tube (stage ii), the magnetic flux across the coils increases on the right side and decreases on the left. Current is then generated in the coils in opposite directions for different sides according to Lenz's law. Meanwhile, the relative displacement between the slider and the PTFE film results in a different inductive potential between the two Cu electrodes, which drives induced electrons to flow from the left electrode to the right electrode, generating a triboelectric current to the left. The electromagnetic and triboelectric currents last until the slider reaches maximum displacement (stage iii). The slider is then pushed back with decreasing displacement by the restoring force of the system (stage iv). The magnetic flux crossing the copper coils decreases on the left side and increases on the right, generating an EMG current opposite that of stage ii. Meanwhile, the potential difference between the two Cu electrodes decreases, and the inductive electrons flow back to the left electrode, forming a triboelectric current to the right. The slider then returns to the initial state and repeats the process on the other side. In this way, the current is constantly generated by the EMG and TENG.

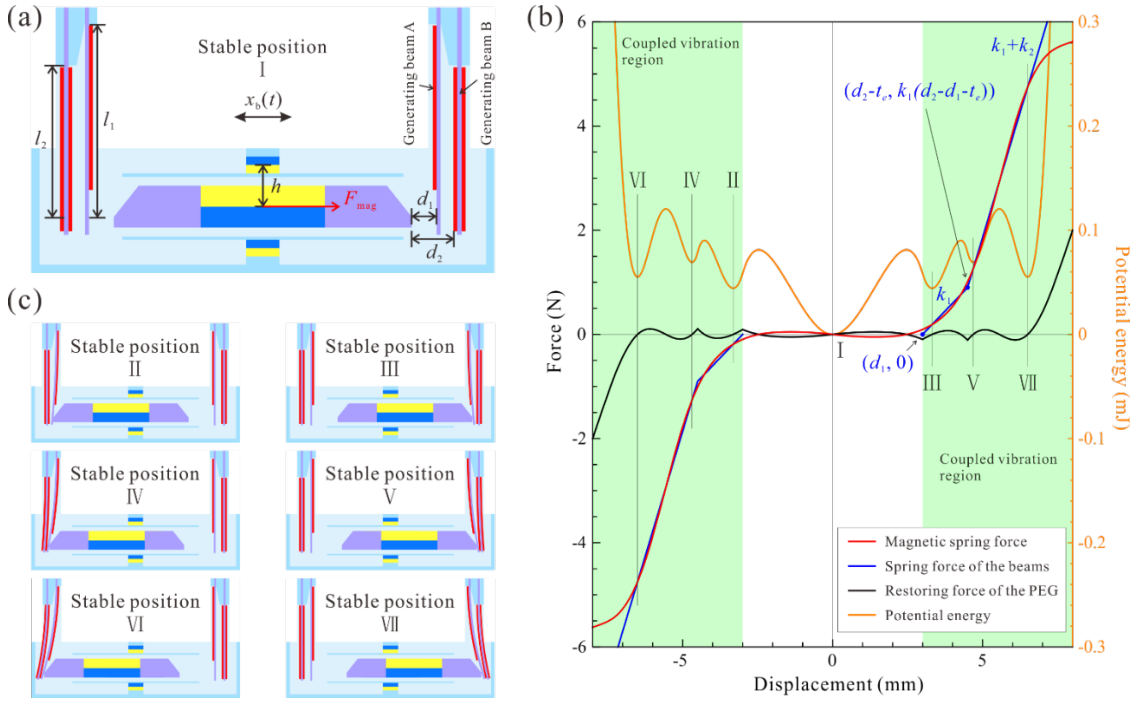

Fig. 2. (a) Schematic drawing of the PEG, (b) the force-displacement curve and the potential energy of the septuple-stable dynamic system, (c) other six stable equilibrium positions of the slider excluding the middle one.

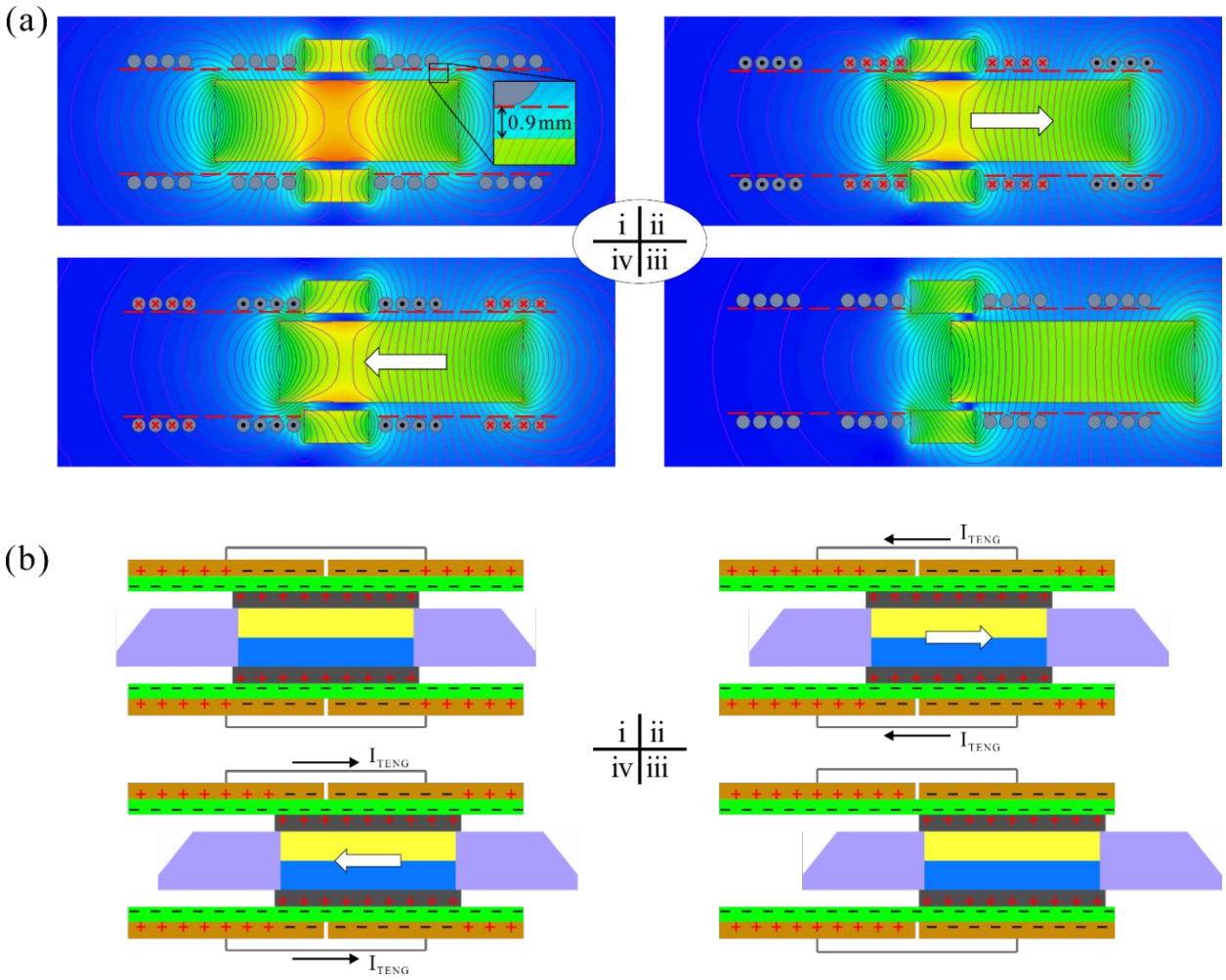

Fig. 3. Schematic diagram showing the power generation process of (a) the EMG and (b) the TENG over a half cycle.

3.2. Theoretical modeling

A lumped parameter model of the proposed tri-hybrid energy harvester under base excitation is shown in Fig. 4(a). When the generator structure is subjected to harmonic base excitation $x_b(t)$ according to the relative displacement of the slider, x, the dynamics of the septuple-stable system can be divided into three cases. In the first case, the relative displacement x does not exceed the critical value of d_1, no collision occurs, and the slider vibrates with a damping of c_t under the action of the magnetic spring force, F_{mag}. All generating beams retain their positions. In the second case, when the relative displacement x exceeds the critical value of d_1 but is less than $d_2 - t_e$, the slider impacts GBA and they vibrate together for a short period with additional stiffness, k_1, and damping, c_1. After separation from GBA, the slider reverts to its original dynamic behavior as in the first case. Meanwhile, GBA vibrates freely at its own resonant frequency until it collides with the slider during the next cycle. In the third case, the relative displacement x exceeds the distance $d_2 - t_e$ during the coupled vibration. GBB impacts the motion combination of the slider and GBA and does a coupled vibration with the

motion combination for a while. In this case, the additional stiffness and damping of the system further increase to $k_1 + k_2$ and $c_1 + c_2$, respectively. After the short period of coupled vibration, GBB separates from the motion combination and freely vibrates at its own resonant frequency until it collides with the combination during the next cycle. Meanwhile, the motion combination reverts to its original motion behavior as in the second case. The piecewise nonlinear governing equations of the proposed tri-hybrid energy harvester can be obtained as

$$\begin{cases} m\ddot{x} + c_t\dot{x} + F_{mag} = -m\ddot{b} & |x| < d_1 \\ m\ddot{x} + (c_t + c_1)\dot{x} + k_1(x - d_1) + F_{mag} = -m\ddot{b} & d_1 < |x| < d_2 - t_e \\ m\ddot{x} + (c_t + c_1 + c_2)\dot{x} + k_1(d_2 - d_1 - t_e) + k_2(x - d_2 + t_e) + F_{mag} = -m\ddot{b} & |x| > d_2 - t_e \end{cases} \quad (1)$$

where m is the proof mass; $b(t) = A\sin(\omega_0 t)$; A is the amplitude of the base excitation; ω_0 is the frequency of the base excitation; and c_t is the total damping coefficient equal to the sum of the electrical and mechanical damping except for the portion of the generating beams. The magnetic spring force on the slider is measured at different relative displacements by a force gauge and fitted as a polynomial, shown as

$$F_{mag} = a_1 x + a_2 x^3 + a_3 x^5 + \cdots + a_n x^{2n-1} \quad (2)$$

where $a_1, a_2, \ldots, a_n$ are polynomial coefficients.

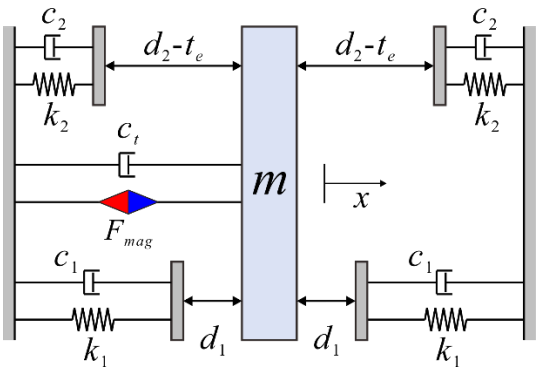

Fig. 4. An equivalent mechanical model of the proposed tri-hybrid energy harvester.

For the PEG, because GBA is composed of an MFC patch and a beryllium bronze plate, it works as a unimorph cantilever beam, whereas GBB with two MFC patches connected in parallel operates as a bimorph cantilever beam. Fig. 5 shows the cross-sectional view of these two kinds of beams. The z-axis is along the length direction, with $z = 0$ located at the fixed end. The x-axis is along the thickness direction, with $x = 0$ at the interface between the beryllium bronze plate and the upper MFC. For GBA, composed of a beryllium bronze plate with Young's modulus E_b, length l_1, width b_{B1}, and thickness t_{B1} and an MFC patch, with Young's modulus E_M, length l_2, width b_M, and thickness t_M, the position of the

neutral axis in the composite region $0 < x < l_1$ can be expressed as [59]

$$t_{n1} = \frac{E_M t_M{}^2 b_M - E_b t_{b1}{}^2 b_{b1}}{2(E_b t_{b1} b_M + E_M t_M b_{b1})} \tag{3}$$

GBB is composed of a beryllium bronze plate with length l_2, width b_{b1}, and thickness t_{b1} and two MFC patches, $t_{n2} = t_{b2}/2$, due to the structural symmetry. The lateral stress on the MFC for GBA and GBB at position (z, x) can be respectively written as

$$\sigma_A(z,x) = \frac{k_1 x_A E_M}{D_{A\text{-}com}}(l_1 - z)(x - t_{n1}) \tag{6}$$

$$\sigma_B(z,x) = \frac{k_2 x_B E_M}{D_{B\text{-}com}}(l_2 - z)(x - \frac{t_{b2}}{2}) \tag{7}$$

where

$$k_1 = \left[(\frac{l_2^3 + 3l_2^2(l_1 - l_2) + 3l_2(l_1 - l_2)^2}{3D_{A\text{-}com}}) + \frac{(l_1 - l_2)^3}{3D_{non}} \right]^{-1} \tag{8}$$

$$k_2 = \frac{3D_{B\text{-}com}}{l_2^3} \tag{9}$$

$$D_{A\text{-}com} = \frac{E_M b_M t_M^3}{12} + \frac{E_b b_{b1} t_{b1}}{12}(4\,t_{b1}^2 + 6t_{b1}t_M + 3t_M^2) \tag{10}$$

$$D_{B\text{-}com} = \frac{E_M b_M t_M^3}{12} + \frac{E_b b_{b2} t_{b2}}{6}(4\,t_{b2}^2 + 6t_{b2}t_M + 3t_M^2) \tag{11}$$

$$D_{non} = \frac{E_b b_{b1} t_{b1}^3}{12} \tag{12}$$

Here, x_A and x_B are the tip displacements of GBA and GBB, respectively, $D_{A\text{-}com}$ and $D_{B\text{-}com}$ are the effective bending moduli of GBA and GBB in the composite region, respectively, and D_{non} is the bending modulus of GBB in the non-composite region ($l_2 < x < l_1$).

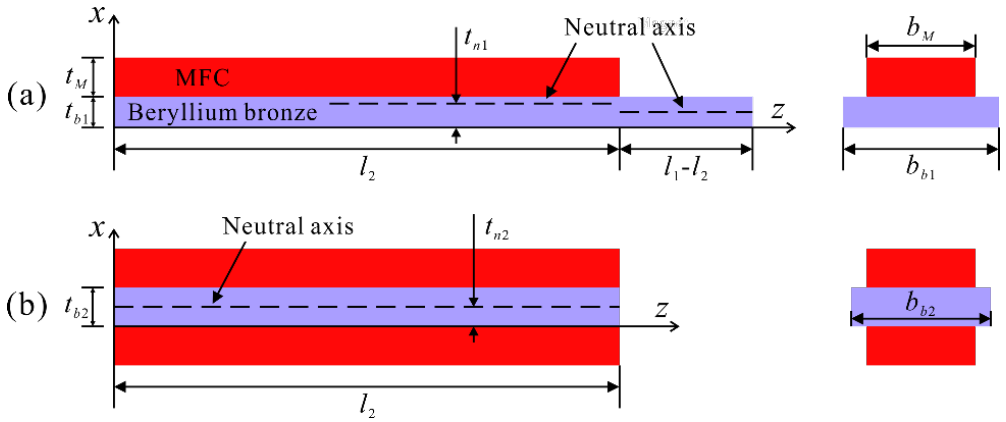

Fig. 5. Schematic cross-sectional view of (a) the unimorph cantilever beam; and (b) the bimorph cantilever beam.

The induced electric fields, $E_A(z, x)$ and $E_B(z, x)$, for GBA and GBB, respectively, in the thickness direction at (z, x) in the MFC patches are

$$E_A(z,x) = (\frac{-d_{31}}{\varepsilon_r \varepsilon_0}) \times \sigma_A(z,x) = -\frac{d_{31} k_1 x_A E_M}{\varepsilon_r \varepsilon_0 D_{A\text{-}com}} (l_1 - z)(x - t_{n1}),\ 0 < z < l_2 \tag{13}$$

$$E_B(z,x) = (\frac{-d_{31}}{\varepsilon_r \varepsilon_0}) \times \sigma_B(z,x) = -\frac{d_{31} k_2 x_B E_M}{\varepsilon_r \varepsilon_0 D_{B\text{-}com}} (l_2 - z)(x - \frac{t_{b2}}{2}),\ 0 < z < l_2 \tag{14}$$

where d_{31}, ε_0, and ε_r are the piezoelectric strain constant, the permittivity of free space, and the dielectric constant of MFC, respectively. Hence, the generated open-circuit voltages of GBA and GBB can be respectively given by

$$V_{oc\text{-}A} = \frac{1}{l_2} \int_0^{l_2} \int_0^{t_M} E_A(z,x) dx dz = -\frac{d_{31} k_1 x_A E_M t_M}{4 \varepsilon_r \varepsilon_0 D_{A\text{-}com}} (2t_{n1} + t_M)(2l_1 - l_2) \tag{15}$$

$$V_{oc\text{-}B} = \frac{1}{l_2} \int_0^{l_2} \int_0^{t_M} E_B(z,x) dx dz = -\frac{l_2 d_{31} k_2 x_B E_M t_M}{4 \varepsilon_r \varepsilon_0 D_{B\text{-}com}} (t_{b2} + t_M) \tag{16}$$

For the EMG, as described by Faraday's Law of electromagnetic induction [1], the relationships of the open-circuit voltage V_{oc} and the short-circuit current I_{sc} can be expressed as

$$V_{oc\text{-}EMG} = -N d\phi / dt \tag{17}$$

$$I_{sc\text{-}EMG} = V_{oc} / R_t \tag{18}$$

where N, ϕ, and R_t are, respectively, the number of turns of a coil, the magnetic flux through the area enclosed by the four coils, and the total internal coil resistance of the four coils.

For the TENG, V_{oc} and I_{sc} can be expressed as follows [60]

$$V_{oc-TENG} = Q_{sc} / C = \Delta S \cdot \sigma / C \tag{19}$$

$$I_{sc-TENG} = dQ_{sc} / dt \tag{20}$$

where Q_{sc}, C, and σ are the short-circuit transferred charge, the capacitance between two electrodes, and the surface charge density on the slider, respectively. Because the transferred charge is induced by the triboelectric charge on the slider, the potential difference between the two electrodes is proportional to the change of contact area, ΔS.

3.3. Shaker test results

The low-frequency tri-hybrid generator was designed to operate within the broad bandwidth of human-induced vibration for powering portable electronics. Thus, the fabricated tri-hybrid generator was tested using both an electrodynamic shaker and manual vibration. Fig. 6 shows the experimental

setup of the electrodynamic shaker test.

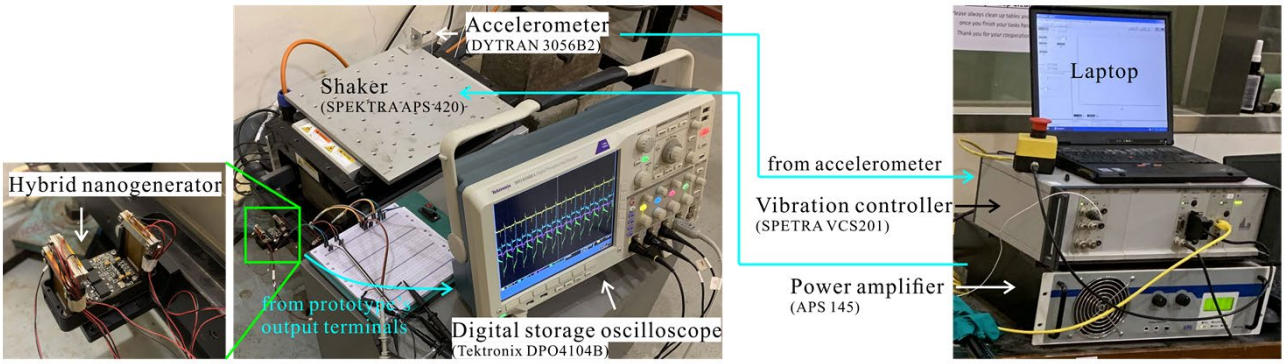

Fig. 6. Experimental setup of the electrodynamic shaker test

Under various base accelerations (0.5 g, 1 g, and 1.5 g), the frequency responses of one GBA, one GBB, the EMG, and the TENG were investigated. The measured peak-peak open-circuit voltages in the frequency range of 2–12.5 Hz are shown in Fig. 7. Because all the generators in the device were driven by the same mechanical oscillation, their voltage responses can exhibit similar broadband resonant behavior due to the septuple-stable nonlinear restoring force of the oscillator. At 0.5g, the generators can produce large peak-peak open-circuit voltages at low frequencies owing to the resonant inter-well oscillations around various local oscillation frequencies. With increasing excitation frequency, the output voltages dropped by around 5 Hz due to the effect of frictional damping, and the generators reached minimum output voltages at 6 Hz (42.9 V for GBA, 36.1 V for GBB, 3.0 V for the EMG, and 37.4 V for the TENG). After 8 Hz, the generators began to exhibit non-resonant behavior, which generally exists in a springless system with rigid boundaries, and the output voltages increased with increasing frequency. Such behavior was induced by the septuple-stable nonlinear restoring force. That is, the restoring force was restricted below an ultralow level (lower than 0.2 N) in the region between the two outermost potential wells, but it increased rapidly when the displacement was beyond that region. By combining the low-frequency resonant inter-well oscillation behavior and the non-resonant behavior, the septuple-stable generator produced large electric outputs in both low-frequency and relatively high-frequency ranges, which covered a continuous broad bandwidth of 2–12.5 Hz for this study. When the acceleration amplitude increased to 1g, the frequency range of the resonant inter-well oscillations extended to 2–10 Hz, whereas the corresponding voltage responses changed more gently. When the acceleration amplitude reached 1.5 g, all the generators do resonant inter-well oscillations with their output voltages increase slowly with frequencies up to 10.5 Hz. Then, with small decreases in their voltage responses, all the generators switched to a non-resonant pattern. The frequency response characteristics of the generators guaranteed high harvesting efficiencies for

different kinds of human body-induced vibrations.

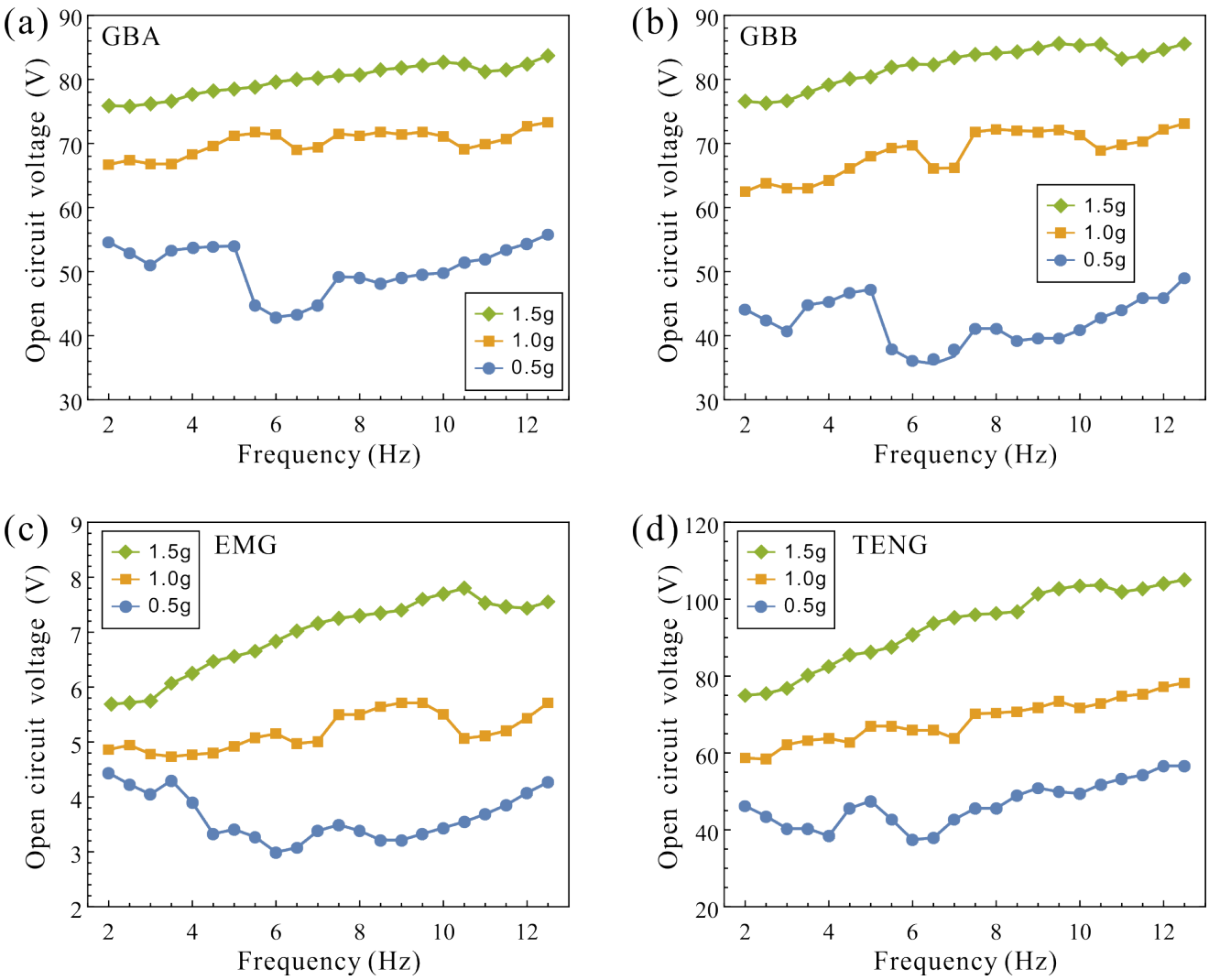

Fig. 7. Measured peak-peak open-circuit voltage of (a) one GBA, (b) one GBB, (c) the EMG, and (d) the TENG against different frequencies under 0.5 g, 1 g and 1.5 g base accelerations using an electrodynamic shaker.

Fig. 8 illustrates the open-circuit voltage and load-circuit current of one GBA, one GBB, the EMG, and the TENG under an excitation frequency of 5 Hz at 1g acceleration provided by the electrodynamic shaker. The output current of each generator unit was measured at load resistances of 135 kΩ, 45 kΩ, 290 Ω, and 20 MΩ. The results show that, even though GBB's deflection was always 1.5 mm less than that of GBA (the value of $d_2 - d_1 - t_e$), GBB produced a peak open-circuit voltage of 57.6 V and a load-circuit current of 701.6 μA, values that were higher than those of GBA (45.6 V and 241.4 μA, respectively) due to the higher electromechanical coupling factor and the unimorph configuration with parallel connection. For the EMG, the peak open-circuit voltage and load-circuit current were 2.85 V

and 5.27 mA, respectively. The TENG produced a high peak open-circuit voltage of 42 V, whereas its load-circuit current was as low as 4.34 μA due to the high internal impedance.

To investigate the output ability of the proposed tri-hybrid energy harvester, the maximum output power of one GBA, one GBB, the EMG, and the TENG were measured and calculated across different external load resistances at 5 Hz under 1g acceleration. As shown in Fig. 9, the voltage across the load increased with increasing load resistance. However, maximum power was delivered when the load resistance matched the source resistance. For one GBA, the obtained maximum power was 7.87 mW under an optimum load resistance of 135 kΩ, whereas the corresponding average power was 0.26 mW. For one GBB, the maximum power and corresponding average power were 22.05 and 0.86 mW, respectively, at an optimum load resistance of 45 kΩ. Because most of the energy is output during the coupled vibration, the matching load resistance for a frequency up-converted harvester was experimentally found to match the high resonant frequency of the generating beam rather than the low excitation frequency [52]. As a consequence, GBB with a higher resonant frequency of 322.6 Hz matched a load resistance less than half that of GBA with a resonant frequency of 155.9 Hz, thereby leading to much higher power generation.

For the EMG, a maximum power of 8.04 mW (corresponding to 2.07 mW average power) was obtained at the matched load of 290 Ω. For the TENG, under a matching load resistance of 20 MΩ, the maximum and average powers were 50 and 3.2 μW, respectively. In the proposed tri-hybrid energy harvester, the EMG has low internal impedance and high current output, whereas the PEG and the TENG have high internal impedance, but they can generate much larger voltages than the EMG. To avoid large internal power consumption when the PEG, EMG, and TENG units are working simultaneously, a rectifier bridge circuit was used to combine the electric output of each unit. Fig. 9(d) shows that the measured hybridized maximum power was 24.16 mW, corresponding to an average power of 2.18 mW under an optimum load resistance of 35 kΩ. In addition, we observe that the hybridized maximum power is significantly reduced when comparing with the algebraic sum of output power generated by all the individual generators. This issue is raised from the impedance mismatch between different contributing parts when a load is added [1]. Additional power management circuits can be utilized to match the output impedance of different working mechanisms and to achieve a better power output performance [61, 62]. In this work, a standard rectifier circuit was utilized in the experimental studies for a direct comparison with other works.

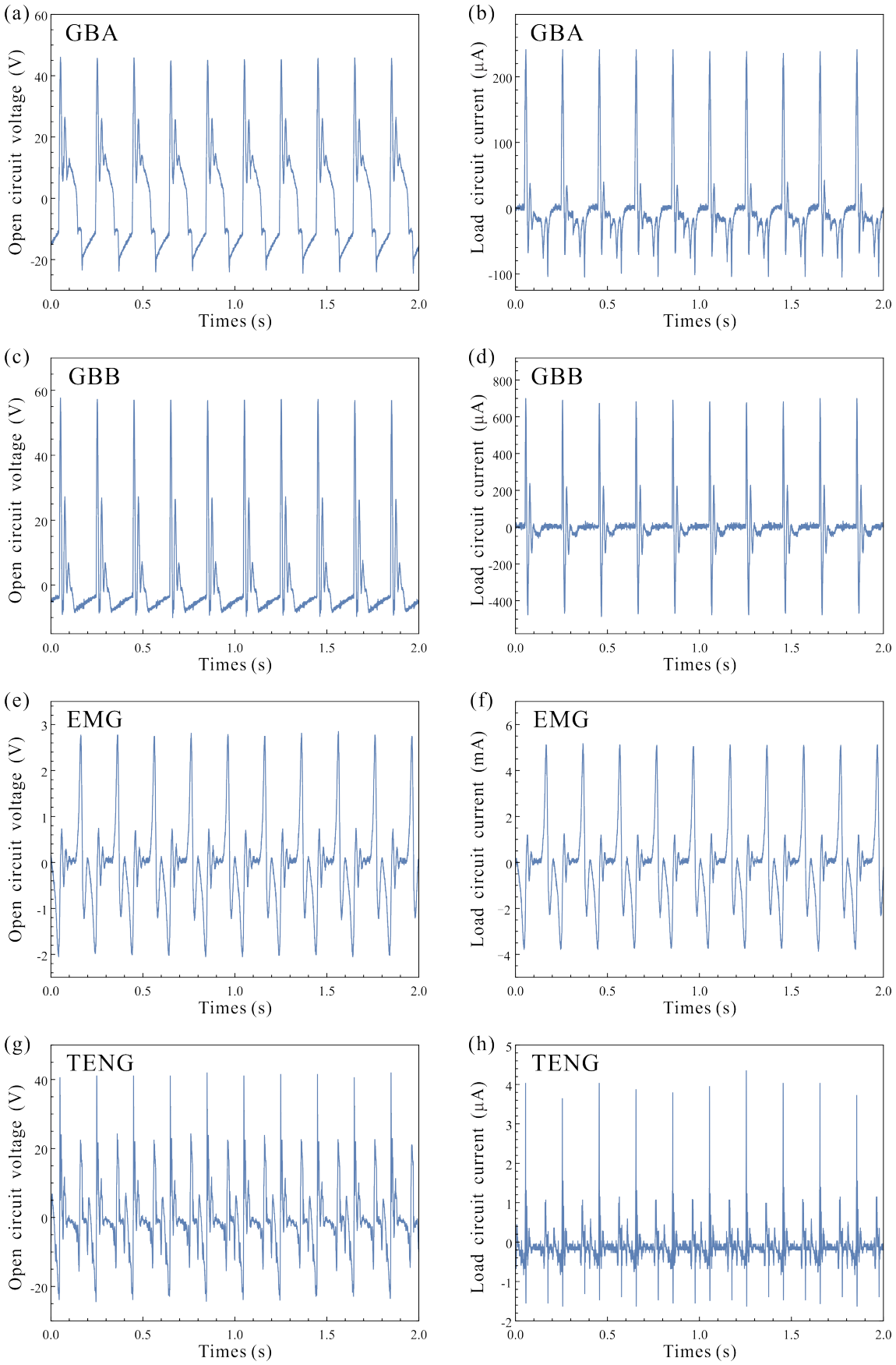

Fig. 8. Measured open-circuit voltage curves and load-current curves of (a, b) GBA, (c, d) GBB, (e, f) EMG, and (g, h) TENG under 5 Hz frequency at 1 g acceleration.

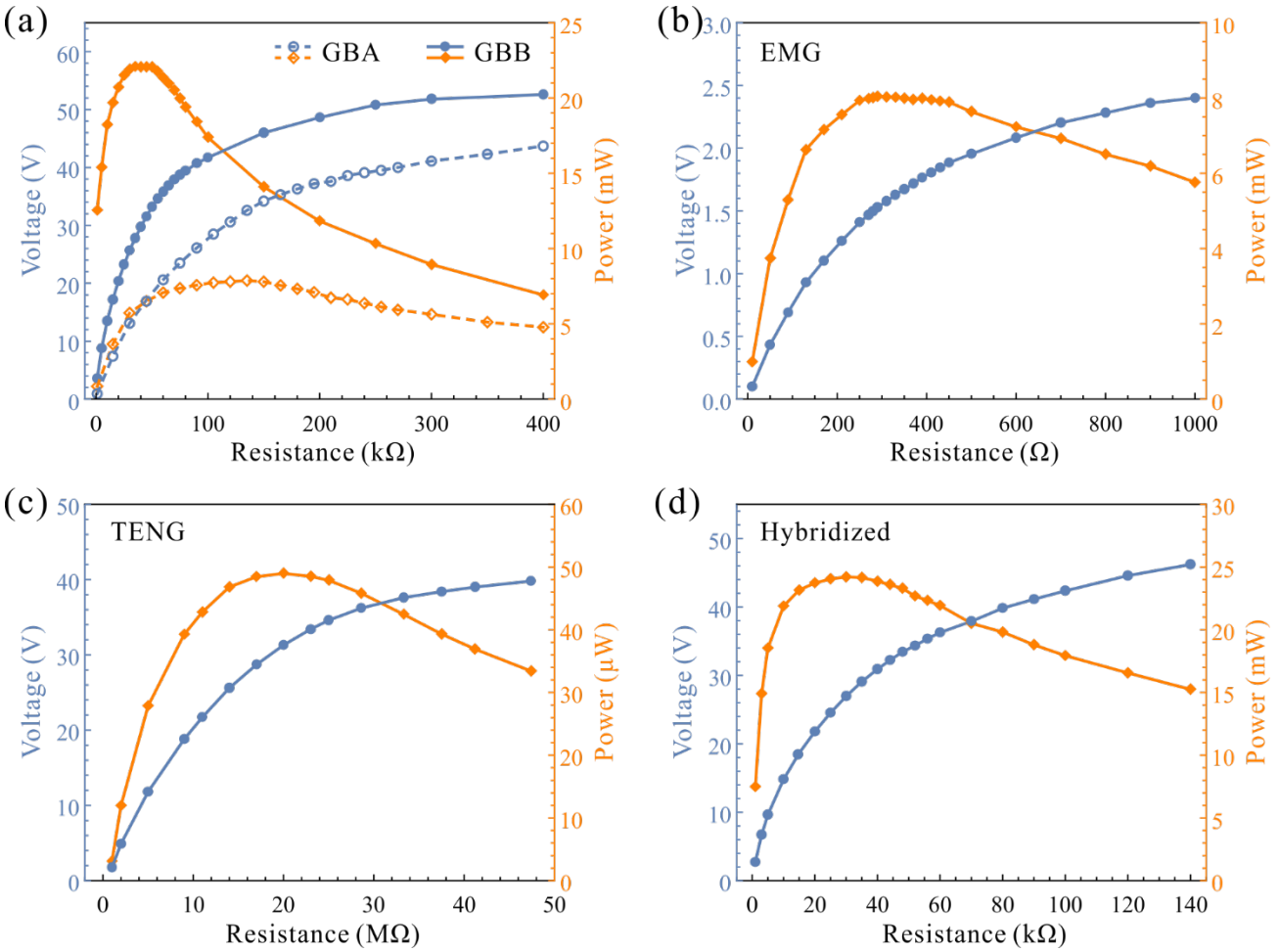

Fig. 9. Dependence of the output voltage and peak output power on the external load resistance for (a) one GBA and one GBB, (b) the EMG, (c) the TENG and (d) the tri-hybrid energy harvester.

3.4. Human motion test results

The output performance of the tri-hybrid energy harvester under various basic human motions such as handshaking, walking, and slow running was evaluated with the device placed in vertical and horizontal positions. The human motion-induced accelerations applied on the device in the X, Y, and Z axes were simultaneously measured by accelerometers. The output power and the charging curves of the tri-hybrid energy harvester for charging a 47-μF capacitor were recorded. For the horizontal and vertical handshaking tests, the results of which are depicted in Fig. 10(a), the three-axis acceleration waveforms (Fig. 10(b)) show that the horizontal handshaking test was primarily controlled along the X axis, with a peak acceleration of ~1.8 g and a frequency of 6.1 Hz, whereas the vertical handshaking test was primarily controlled along the Z axis, with a peak acceleration of ~2 g and a frequency of 5.7 Hz. Under the horizontal and vertical handshaking activities, the instantaneous peak powers of the harvester at matching load resistances were 38.5 and 42.7 mW, respectively. In addition, Fig. 10(c) shows that the capacitor was charged up to 35 V in 15 s and up to 30 V in 27 s from the horizontal and

vertical handshaking tests, respectively. Comparing the power levels and charging levels provided by the tri-hybrid energy harvester during the handshaking tests, the harvester exhibited a higher power level but a lower charging level for the vertical test. In the case of vertical handshaking, due to the effect of gravity and the irregular excitation, the impact on the lower generating beams was enhanced, whereas the impact on the upper generating beams was weakened. In the case of horizontal handshaking, the slider efficiently impacted the generating beams on both sides periodically, which, in turn, generated more power for capacitance charging.

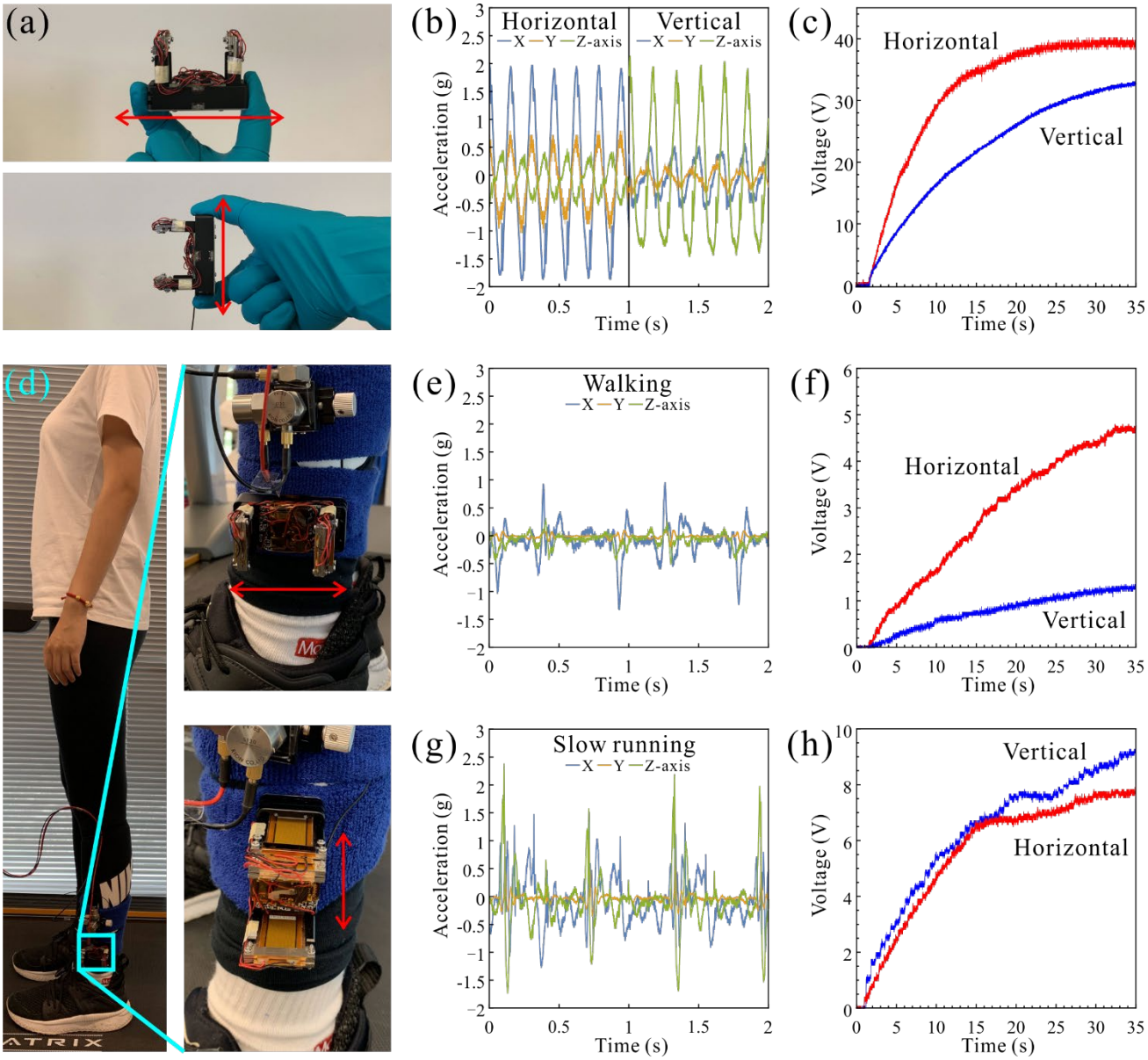

Fig. 10. Demonstration of the tri-hybrid energy harvester under various basic human motions. (a) Photograph of the prototype in horizontal and vertical handshaking tests. (b) Acceleration waveforms measured in horizontal and vertical handshaking tests. (c) Measured voltage of a 47 μF capacitor charged by the prototype during the horizontal and vertical handshaking tests. (d) Photographs of the

walking and slow running test with the prototype tied up on the calf in the horizontal and vertical position. (e, g) Acceleration waveforms measured in walking and slow running tests, respectively. (f, h) Measured voltage of a 47 μF capacitor charged by the prototype placed in the horizontal and vertical position during the walking and slow running tests, respectively.

For the tests of walking (5 km/h) and slow-running (8 km/h) on a treadmill, the tri-hybrid energy harvester was tied in horizontal and vertical positions on a person's calf, as shown in Fig. 10(d). The measured acceleration waveforms (Figs. 10(e) and (g)) show that the walking motion was primarily generated along the X axis (peak acceleration of ~1.3g, dominant frequency of 2.5 Hz), whereas the slow running motion was primarily generated along the X axis (peak acceleration of ~1.5 g, dominant frequency of 3.5 Hz) and the Z axis (peak acceleration of ~2.2 g, dominant frequency of 3.5 Hz). The instantaneous peak powers of the harvester were 24.5 mW (walking, horizontal), 10.2 mW (walking, vertical), 27.2 mW (slow running, horizontal), and 33.1 mW (slow running, vertical). Fig. 10(f) shows that the capacitor was charged up to 4.7 V in 35 s and up to 1.3 V in 35 s from walking with the harvester placed in the horizontal and vertical positions, respectively.

For slow running, the capacitor was charged from 0 to 6.6 V in 17 s for the horizontal position and from 0 to 7.7 V in 20 s for the vertical position. From the human motion tests, it can be concluded that the best output power performance of the tri-hybrid energy harvester was obtained from horizontal handshaking and slow running vibration activities (the horizontal and vertical positions exhibited similar performance).

3.5. Application to electronic devices

Because most low-power electronics run on DC voltage/current, the alternating current (AC) waveforms generated by the harvester units need to be rectified and stored in an energy-storage unit, such as a capacitor or a battery. A schematic diagram of the charging circuit for the tri-hybrid energy harvester is shown in Fig. 11(a), in which the six rectifier ICs (DB101S) were connected to the generators. Then, the rectified DC voltage from the generators were connected to a ceramic capacitor/load in parallel. To avoid the problem of internal power consumption, full wave rectifier bridges were connected to each of the generators to rectify the output voltage from AC to DC, as shown in Fig. 11(a). Then, the worst case that the output voltages of different mechanisms are in opposite phase can be prevented. The DC outputs were connected in parallel to a capacitor. Generally, factors that can affect the energy storage efficiency are the output impedance and the voltage matching. The phase delay may not affect the energy storage efficiency in this case. For most of the hybrid energy harvesters proposed recently, the AC outputs of various generator units are not in phase. They adopted

full wave rectifier bridges to address the issue of internal power consumption. To reduce the energy loss caused by rectifiers, some researchers designed the generator units in phase, e.g., Refs. [1] and [61]. Then, different generator units can be directly connected without rectifiers, the power management circuit is also simplified.

To demonstrate that the tri-energy harvester is an efficient energy/power source, the output of the hybrid harvester was used to power (by handshaking and slow running) an electronic humidity/temperature meter with a 100 μF capacitor connected in parallel. The charging–discharging characteristics of this 100 μF capacitor under handshaking is illustrated in Fig. 11(b). The electronic humidity/temperature meter turned on when the storage capacitor was charged up to 1.3 V after 1 s and kept running for as long as the harvester was being excited. When the handshaking stopped, the electronic humidity/temperature meter remained on until the capacitor voltage dropped to 0.85 V at 18 s. Similarly, a handshaking demonstration with various vibration frequencies was recorded and is shown in Video 1. The hybrid harvester's ability to power the electronic humidity/temperature meter under slow running is demonstrated in Fig. 11(c) and Video 2. In addition, by handshaking, the hybrid harvester successfully powered a commercial triaxial accelerometer ADXL335 (Fig. 11(d) and Video 3) and simultaneously lit up 80 LEDs (Fig. 11(e) and Video 4).

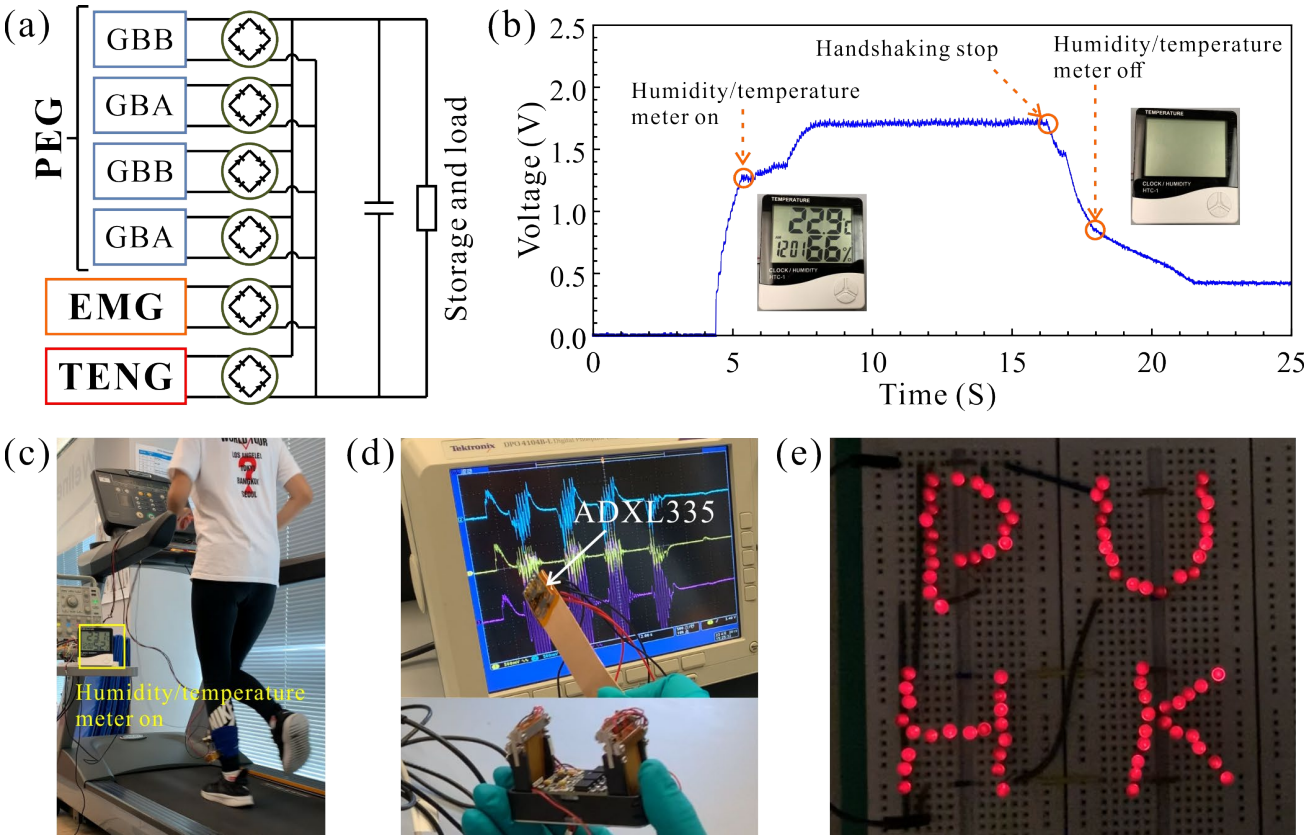

Fig. 11. (a) Schematic configuration of the tri-hybridized energy harvester circuit. (b) Charging-

discharging behavior of a 100 μF capacitor with an electronic humidity/temperature meter acting as a load. (c) The proposed device successfully powers the electronic humidity/temperature meter under slow running. (d) A triaxial accelerometer ADXL335 powered by the device under handshaking. (e) LEDs.

3.6. Performance comparison

A performance comparison between the proposed tri-hybrid energy harvester and recently reported low-frequency hybrid energy harvesters [2, 37, 39, 44, 49, 57] is shown in Table 1. Because the prototype was fabricated on a macroscale, the comparison was carried out with similar devices. The comparison shows that, for low-frequency vibration energy harvesting, our proposed device exhibits outstanding performance compared to other reported devices in terms of both the operation bandwidth and the power density. The proposed tri-hybrid energy harvester offers a novel septuple-stable dynamic system, which not only combines low-frequency resonant inter-well oscillation behavior and the non-resonant behavior to produce a broad bandwidth, it also enhances the output performance of the frequency up-conversion technique, consequently increasing the power density. The tri-hybrid energy harvester is designed for human body-induced motion-based applications, and it offers a high-efficiency operating bandwidth that can cover the vibration frequencies of general human motion. In terms of durability, we kept our prototype harvester under experiments for a long time, no significant damage of the generating beams or magnetic slider was observed.

Table 1. Comparison of the proposed tri-hybrid energy harvester with other works reported recently.

Reference (Types)	Bandwidth (Hz)	Operating conditions	Peak power (mW)	Power density (W/m^3)
Ref. [2] (EM + TE)	4 – 12	6 Hz, 1 g	5.41	395.4
Ref. [37] (PE + EM)	6 – 8.5	6 Hz, 1.5 g	1.41	36.4
Ref. [39] (EM + TE)	46 – 114	80 Hz, 2 g	5.02×10^{-2}	0.8
Ref. [44] (EM + TE)	3.5 – 5	4.5 Hz, 0.6 g	10.07	344
Ref. [49] (PE + EM + TE)	10 – 31.5	20 Hz, 0.5 g	3.46×10^{-2}	5.4
Ref. [57] (EM + TE)	22	22 Hz, 1 g	19.8	167.2
This work (PE + EM + TE)	2 – 12.5	5 Hz, 1 g	24.16	700.3

g = 9.8 m/s^2, PE = piezoelectric, EM = electromagnetic, TE = triboelectric.

4. Conclusions

In this work, we designed, fabricated, and tested a low-frequency, broadband, tri-hybrid energy harvester with septuple-stable nonlinearity-enhanced mechanical frequency up-conversion mechanism

to scavenge significant power from various human body-induced vibrations to power portable electronics. Under the electrodynamic shaker test, the prototype exhibited a broad bandwidth of 2–12.5 Hz, which covers the vibration frequencies of general human motion, and delivered a high output power of 24.16 mW, corresponding to a power density of 700.3 W/m^3 across a loading resistance of 35 kΩ under 5 Hz frequency at 1g acceleration. For various basic human motions such as handshaking, walking, and slow running, the prototype generated output powers of 38.5, 24.5, and 27.2 mW, respectively, in the horizontal position and 42.7, 10.2, and 33.1 mW, respectively, in the vertical position. The best output power performance was obtained from horizontal handshaking and slow running motions. Moreover, we demonstrated the powering of a tri-axial accelerometer and a humidity/temperature meter from handshaking and slow-running motions. The prototype exhibited a wider bandwidth and a much higher power density than similar devices reported recently. This work makes significant progress toward hybrid energy harvesting from various human motions and its potential application for powering portable electronics.

Future research will focus on the design of an advanced power management circuit to match the output impedance of different working mechanisms, and a voltage matching circuit for efficient energy storage. With the assistance of these new design circuits, it is expected that not only the tri-hybrid energy harvester can take the advantages of the newly proposed multi-stable nonlinearity-enhanced mechanical frequency up-conversion mechanism, and also it can work well in perpendicular direction and in alignment under the gravity field effect to maintain its efficiency under the high bandwidth and low required acceleration.

Acknowledgements

The work described in this paper was supported by the Early Career Scheme (Project No. PolyU 252026/16E) and the Research Impact Fund (Project No. R-5020-18) from the Research Grants Council of the Hong Kong Special Administrative Region. The funding support from the Innovation and Technology Commission of the HKSAR Government to the Hong Kong Branch of National Rail Transit Electrification and Automation Engineering Technology Research Center (Grant No. K-BBY1) is also gratefully acknowledged.

References

[1] J.Y. Hu, S. Niu, W. Wu, Z.L. Wang, Hybridizing triboelectrification and electromagnetic induction effects for high-efficient mechanical energy harvesting, ACS Nano 8 (2014) 7442–7450.

[2] Md Salauddin, R.M. Toyabur, P. Maharjan, M.S. Rasel, J.W. Kim, H. Cho, J.Y. Park, Miniaturized springless hybrid nanogenerator for powering portable and wearable electronic devices from human-body-induced vibration, Nano Energy 51 (2018) 61–72.

[3] K.A. Cook-Chennault, N. Thambi, A. Sastry, Powering MEMS portable devices-A review of non-regenerative and regenerative power supply system with special emphasis on piezoelectric energy harvesting systems, Smart Materials and Structures 17 (2008) 043001.

[4] X. Pu, W. Hu, Z.L. Wang, Toward wearable self-charging power systems: The integration of energy-harvesting and storage devices, Small 14 (2018) 1613–6829.

[5] S.H. Collins, M.B. Wiggin, G.S. Sawicki, Reducing the energy cost of human walking using an unpowered exoskeleton, Nature 522 (2015) 212–215.

[6] J. Wang, S. Li, F. Yi, Y. Zi, J. Lin, X. Wang, Y. Xu, Z.L. Wang, Sustainably powering wearable electronics solely by biomechanical energy, Nature Communications 7 (2016) 12744.

[7] A. Erturk, D.J. Inman, Piezoelectric Energy Harvesting, 2011 (Wiley: Chichester, UK).

[8] X. Li, V. Strezov, Modelling piezoelectric energy harvesting potential in an educational building, Energy Conversion and Management 85 (2014) 435–442.

[9] A. Keshmiri, N. Wu, Q. Wang, A new nonlinearly tapered FGM piezoelectric energy harvester, Engineering Structures 173 (2018) 52–60.

[10] C. Wang, Q.C. Zhang, W. Wang, J.J. Feng, A low-frequency, wideband quad-stable energy harvester using combined nonlinearity and frequency up-conversion by cantilever-surface contact, Mechanical Systems and Signal Processing 112 (2018) 305–318.

[11] S.K. Lai, C. Wang, L.H. Zhang, A nonlinear multi-stable piezomagnetoelastic harvester array for low-intensity, low-frequency, and broadband vibrations, Mechanical Systems and Signal Processing 122 (2019) 87–102.

[12] J.M. Donelan, Q. Li, V. Naing, J.A. Hoffer, D.J. Weber, A.D. Kuo, Biomechanical energy harvesting generating electricity during walking with minimal user effort, Science 319 (2008) 807–810.

[13] W. Wang, J. Cao, N. Zhang, J. Lin, W.H. Liao, Magnetic-spring based energy harvesting from human motions: Design, modeling and experiments, Energy Conversion and Management 132 (2017) 189–197.

[14] C. Chen, L.Y. Chau, W.H. Liao, A knee-mounted biomechanical energy harvester with enhanced efficiency and safety, Smart Materials and Structures 26 (2017) 065027.

[15] M.A. Halim, R. Rantz, Q. Zhang, L. Gu, K. Yang, S. Roundy, An electromagnetic rotational energy harvester using sprung eccentric rotor, driven by pseudo-walking motion, Applied Energy 217 (2018) 66–74.

[16] L.G.W. Tvedt, D.S. Nguyen, E. Halvorsen, Nonlinear behavior of an electrostatic energy harvester under wide- and narrowband excitation, Journal of Microelectromechanical Systems 19 (2010) 305–316.

[17] Y. Lu, F. Cottone, S. Boisseau, A nonlinear MEMS electrostatic kinetic energy harvester for human-powered biomedical devices, Applied Physics Letters 107 (2015) 253902.

[18] F. Fan, Z. Tian, Z.L. Wang, Flexible triboelectric generator, Nano Energy 1 (2012), 328-334.

[19] Z.L. Wang, Triboelectric nanogenerators as new energy technology for self-powered systems and as active mechanical and chemical sensors, ACS Nano 7 (2013) 9533–9557.

[20] S. Wang, L. Lin, Y. Xie, Q. Jing, S. Niu, Z.L. Wang, Sliding-triboelectric nanogenerators based on in-plane charge-separation mechanism, Nano Letter 13 (2013) 2226–2233.

[21] W. Yang, J. Chen, G. Zhu, J. Yang, P. Bai, Y. Su, Q. Jing, X. Cao, Z.L. Wang, Harvesting energy from the natural vibration of human walking, ACS Nano, 7 (2013) 11317–11324.

[22] W. Yang, J. Chen, Q. Jing, J. Yang, X. Wen, Y. Su, G. Zhu, P. Bei, Z.L. Wang, 3D stack integrated triboelectric generator for harvesting vibration energy, Advanced Functional Materials, 24 (2014) 4090–4096.

[23] K. Parida, V. Kumar, W. Jiangxin, V. Bhavanasi, R. Bendi, P.S. Lee, Highly transparent, stretchable, and self-healing ionic-skin triboelectric nanogenerators for energy harvesting and touch applications, Advanced Materials 29 (2017) 1702181.

[24] Z.L. Wang, T. Jiang, L. Xu, Toward the blue energy dream by triboelectric nanogenerator networks, Nano Energy 39 (2017) 9–23.

[25] D. Kim, S. Lee, Y. Ko, C.H. Kwon, J. Cho, Layer-by-layer assembly-induced triboelectric nanogenerators with high and stable electric outputs in humid environments, Nano Energy 44

(2018) 228–239.

[26] C. Park, S. Yu, S.M. Cho, G. Song, Y. Lee, H.S. Kang, S.W. Lee, H. Eoh, C. Park, Triboelectric nanogenerators with transfer-printed arrays of hierarchically dewetted microdroplets, Nano Energy 51 (2018) 588–596.

[27] H. Guo, X. Pu, J. Chen, Y. Meng, M.-H. Yeh, G. Liu, Q. Tang, B. Chen, D. Liu, Song. Qi, C. Wu, C. Hu, J. Wang, Z.L. Wang, A highly sensitive, selfpowered triboelectric auditory sensor for social robotics and hearing aids, Science Robotics 3 (2018) eaat2516.

[28] G. Liu, J. Chen, Q. Tang, L. Feng, H. Yang, J. Li, Y. Xi, X. Wang, C. Hu, Wireless electric energy transmission through various isolated solid media based on triboelectric nanogenerator, Advanced Energy Materials 8 (2018) 1703086.

[29] T.V. Büren, P.D. Mitcheson, T.C. Green, E.M. Yeatman, A.S. Holmes, G. Tröster, Optimization of inertial micropower generators for human walking motion, Sensors 6 (2006) 28–38.

[30] H. Külah, K. Najafi, Energy scavenging from low-frequency vibrations by using frequency up-conversion for wireless sensor applications, IEEE Sensors Journal 8(2008) 261–268.

[31] M.A. Halim, H. Cho, M. Salauddin, J.Y. Park, A miniaturized electromagnetic vibration energy harvester using flux-guided magnet stacks for human-body-induced motion, Sensors and Actuators A 249 (2016) 23–31.

[32] L. Gu, Low-frequency piezoelectric energy harvesting prototype suitable for the MEMS implementation, Microelectronics Journal 42 (2011) 277–282.

[33] K. Zhang, X. Wang, Y. Yang, Z.L. Wang, Hybridized electromagnetic-triboelectric nanogenerator for scavenging biomechanical energy for sustainably powering wearable electronics, ACS Nano 9 (2015) 3521–3529.

[34] U. Javed, A. Abdelkefi, Role of the galloping force and moment of inertia of inclined square cylinders on the performance of hybrid galloping energy harvesters, Applied Energy 231 (2018) 259–276.

[35] H. Rawnak, R.Y. Mehmet, A wearable energy harvester unit using piezoelectric-electromagnetic hybrid technique, Sensors and Actuators A 257 (2017) 198–207.

[36] R. Sriramdas, R. Pratap, An experimentally validated lumped circuit model for piezoelectric and electrodynamic hybrid harvesters, IEEE Sensors Journal 18 (2018) 2377–2384.

[37] K.Q. Fan, S.H. Liu, H.Y. Liu, Y.M. Zhu, W.D. Wang, D.X. Zhang, Scavenging energy from ultra-low frequency mechanical excitations through a bi-directional hybrid energy harvester, Applied Energy 216 (2018) 8–20.

[38] R.M. Toyabur, M. Salauddin, H. Cho, J.Y. Park, A multimodal hybrid energy harvester based on piezoelectric-electromagnetic mechanisms for low-frequency ambient vibrations, Energy Conversion And Management 168 (2018) 454–466.

[39] R.K. Gupta, Q. Shu, L. Dhakar, T. Wang, C. H. Heng, C. Lee, Broadband energy harvester using non-linear polymer spring and electromagnetic/triboelectric hybrid mechanism, Scientific Reports 7 (2017) 41396.

[40] T. Quan, X. Wang, Z.L. Wang, Y. Yang, Hybridized electromagnetic-triboelectric nanogenerator for a self-powered electronic watch, ACS Nano 9 (2015) 12301–12310.

[41] M.L. Seol, J.W. Han, S.J. Park, Hybrid energy harvester with simultaneous triboelectric and electromagnetic generation from an embedded floating oscillator in a single package, Nano Energy 23 (2016) 50–59.

[42] M.L. Seol, S.B. Jeon, J.W. Han, Ferrofluid-based triboelectric-electromagnetic hybrid generator for sensitive and sustainable vibration energy harvesting, Nano Energy 31 (2017) 233–238.

[43] J.X. Zhu, A.C. Wang, H.B. Hu, H. Zhu, Hybrid electromagnetic and triboelectric nanogenerators with multi-impact for wideband frequency energy harvesting, Energies 10 (2017) 2024.

[44] Md Salauddin, R.M. Toyabur, P. Maharjan, M.S. Rasel, J.W. Kim, H. Cho, J.Y. Park, High performance human-induced vibration driven hybrid energy harvester for powering portable electronics, Nano Energy 45 (2018) 236–246.

[45] Z. Saadatnia, E. Esmailzadeh, H.E. Naguib, Design, simulation, and experimental characterization of a heaving triboelectric-electromagnetic wave energy harvester, Nano Energy 50 (2018) 281–290.

[46] S.C. Karumuthil, S.P. Rajeev, S. Varghese, Piezo-tribo nanoenergy harvester using hybrid polydimethyl siloxane based nanocomposite, Nano Energy 40 (2017) 487–494.

[47] Y.B. Guo, X.S. Zhang, Y. Wang, W. Gong, Q.H. Zhang, H.Z. Wang, J Brugger, All-fiber hybrid piezoelectric-enhanced triboelectric nanogenerator for wearable gesture monitoring, Nano Energy 48 (2018) 152–160.

[48] Z.J. Li, Z. Saadatnia, Z.B. Yang, H. Naguib, A hybrid piezoelectric-triboelectric generator for low-frequency and broad-bandwidth energy harvesting, Energy Conversion And Management 174 (2018) 188–197.

[49] X.M. He, Q. Wen, Y.F. Sun, Z.Y. Wen, A low-frequency piezoelectric-electromagnetic-triboelectric hybrid broadband vibration energy harvester, Nano Energy 40 (2017) 300–307.

[50] M.A. Halim, H.C.M. Salauddin, J.Y. Park, A miniaturized electromagnetic vibration energy harvester using flux-guided magnet stacks for human-body-induced motion, Sensors and Actuators A 249 (2016) 23–31.

[51] I. Izadgoshasb, Y.Y. Li, N. Lake, L.H. Tang, R.V. Padilla, T. Kashiwao, Optimizing orientation of piezoelectric cantilever beam for harvesting energy from human walking, Energy Conversion And Management 161 (2018) 66–73.

[52] M.A. Halim, J.Y. Park, Modeling and experiment of a handy motion driven, frequency up-converting electromagnetic energy harvester using transverse impact by spherical ball, Sensors and Actuators A 229 (2015) 50–58.

[53] M. Renaud, P. Fiorini, R.V. Schaijk, C.V Hoof, Harvesting energy from the motion of human limbs: the design and analysis of an impact-based piezoelectric generator, Smart Materials and Structures 18 (2009) 035001.

[54] K.L. Li, Q.S. He, J.C. Wang, Z.G. Zhou, X.X. Li, Wearable energy harvesters generating electricity from low-frequency human limb movement, Microsystems & Nanoengineering 4 (2018) 24.

[55] L. Gu, C. Livermore, Impact-driven, frequency up-converting, coupled vibration energy harvesting device for low frequency operation, Smart Materials and Structures 20 (2011) 045004.

[56] C. Wang, Q.C. Zhang, W. Wang, Low-frequency wideband vibration energy harvesting by using frequency up-conversion and quin-stable nonlinearity, Journal of Sound and Vibration 399 (2017) 169–181.

[57] L. Jin, J. Chen, B. Zhang, W. Deng, L. Zhang, H. Zhang, X. Huang, M. Zhu, W. Yang, Z. L. Wang, Self-powered safety helmet based on hybridized nanogenerator for emergency, ACS Nano 10 (2016) 7874–7881.

[58] S. Priya, D.J. Inman, Energy Harvesting Technologies, 2009, (Springer, Boston, US)

[59] X. Li, J.S. Vartuli, D.L. Milius, I.A. Aksay, W.Y. Shih, W.H. Shih, Electromechanical properties of a ceramic d31-gradient flex tensional actuator, Journal of the American Ceramic Society 84 (2001) 996–1003.

[60] S. Niu, Y. Liu, X. Chen, S. Wang, Y.S. Zhou, L. Lin, Y. Xie, Z.L. Wang, Theory of freestanding triboelectric-layer-based nanogenerators, Nano Energy 12 (2015) 760–774.

[61] R. Cao, T. Zhou, B. Wang, Y. Yin, Z. Yuan, C. Li, Z.L. Wang, Rotating-sleeve triboelectric–electromagnetic hybrid nanogenerator for high efficiency of harvesting mechanical energy, ACS Nano 11 (2017) 8370–8378.

[62] X. Wang, Y. Yang, Effective energy storage from a hybridized electromagnetic-triboelectric nanogenerator, Nano Energy 32 (2017) 36–41.